

LATERAL ACCELERATION CONTROL DESIGN OF A NON-LINEAR HOMING MISSILE

T. Sreenuch, A. Tsourdos, E. J. Hughes and B. A. White

*Department of Aerospace, Power and Sensors
Cranfield University - RMCS
Shrivenham, Swindon, SN6 8LA, UK*

Abstract: This paper presents the lateral acceleration control design of non-linear missile model using the multiple single objective Pareto sampling method. The LTI controller design for the uncertain plants is carried out by minimising gain-phase margin and tracking frequency domain based performance objectives. The Pareto optimal solutions (corresponding to a given set of weight vectors) are obtained. The selected solution, as illustration, is analysed. The gain-scheduling controller is obtained by the interpolation of zeros, poles and gains, where the smooth deterministic transition rule is implemented using the TS fuzzy model. The non-linear simulation results show that the selected interpolated controller is a robust tracking controller for all perturbation vertices. ©2004 IFAC

Keywords: Evolutionary Algorithms, Multi-Objective Optimisation, Frequency Domains, Fuzzy Logic, Missiles

1. MISSILE MODEL AND AUTOPILOT REQUIREMENTS

1.1 Non-Linear Model

The missile model used in this study is taken from Horton's MSc thesis (Horton, 1992). It describes a 5 DOF model in parametric format with severe cross-coupling and non-linear behaviour. This study will look at the reduced problem of a 2 DOF controller for the lateral motion (on the xy plane in Fig. 1). The

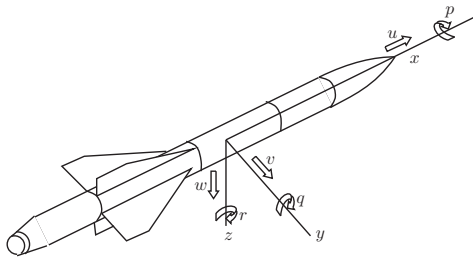


Fig. 1. Airframe axes and nomenclature.

airframe is roll stabilised ($\lambda = 45^\circ$), and no coupling

is assumed between pitch and yaw channels. With these assumptions, the equations of motion are given by

$$\begin{aligned} \dot{v} &= y_v(M, \sigma)v + y_\zeta(M, \sigma)\zeta - Ur, \\ &= \frac{1}{2m}\rho V S(C_{y_v}v + VC_{y_\zeta}\zeta) - Ur, \end{aligned} \quad (1)$$

$$\begin{aligned} \dot{r} &= n_v(M, \sigma)v + n_r(M, \sigma)r + n_\zeta(M, \sigma)\zeta, \\ &= \frac{1}{2I_z}\rho V S d(C_{n_v}v + \frac{1}{2}dC_{n_r}r + VC_{n_\zeta}\zeta), \end{aligned} \quad (2)$$

$$a_y = \dot{v} + Ur, \quad (3)$$

where v the lateral velocity, r the body rate, ζ the rudder fin deflections, U the forward velocity and a_y the lateral acceleration at the centre of gravity *c.g.* are defined in figure 1. y_v, y_ζ are semi-non-dimensional force derivatives due to lateral velocity and fin deflection. n_v, n_r, n_ζ are semi-non-dimensional force derivatives due to lateral velocity, body rate and fin deflection. The aerodynamic derivative $C_{y_v}, C_{y_\zeta}, C_{n_v}, C_{n_r}$ and C_{n_ζ} are the function of Mach number M and incidence angle σ ($\approx v/U$ for $U \gg v$). They are eval-

uated by interpolating the discrete data points obtained from the wind tunnel experiments. These interpolated formulas and other relevant physical parameters are summarised in table 1 and 2.

Symbol	Meaning	Value
a	Speed of sound	340 m/s
ρ	Air density	1.23 kg/m ³
d	Reference diameter	0.2 m
S	Reference area	0.0314 m ²
m	Mass	150 kg full 100 kg all burnt
I_z	Lateral inertia	75 kg · m ² full 60 kg · m ² all burnt
x_{cg}	Centre of gravity	1.3 + $m/50$
x_{cp}	Centre of pressure	1.3 + 0.1 M + 0.3 $ \sigma $
x_f	Fin centre of pressure	2.6 m
s_m	Static margin	$(x_{cg} - x_{cp})/d$
s_f	Fin moment arm	$(x_{cg} - x_f)/d$

Table 1. Physical parameters.

Corresponding force or moment	Aerodynamic derivative	Interpolated formula
Side force	C_{y_v}	$-26 + 1.5M - 60 \sigma $
	C_{y_ζ}	$10 - 1.4M + 1.5 \sigma $
Yawing moment	C_{n_r}	$-500 - 30M + 200 \sigma $
	C_{n_v}	$s_m C_{y_v}$
	C_{n_ζ}	$s_f C_{y_\zeta}$

Table 2. Aerodynamic derivatives.

1.2 Airframe Transfer Function

By linearising the state and output equation (1)-(3) about an operating point gives body rate and acceleration transfer functions of

$$P_{r_\zeta}(s) = \frac{n_\zeta s - (n_\zeta y_v - n_v y_\zeta)}{s^2 - (y_v + n_r)s + (U n_v + y_v n_r)}, \quad (4)$$

$$P_{a_{y_\zeta}}(s) = \frac{y_\zeta s^2 - y_\zeta n_r s - U(n_\zeta y_v - n_v y_\zeta)}{s^2 - (y_v + n_r)s + (U n_v + y_v n_r)}. \quad (5)$$

The weathercock mode is given by the denominator of equation (4) and (5) and, with typical semi-non-dimensional derivatives, shows the polynomial to be lightly damped with a weathercock frequency that is dominated by the term $U n_v$ (Horton, 1995).

1.3 Autopilot Configuration

The lateral autopilot configuration used in this paper is shown in Fig. 2, where $F(s) = \frac{98700}{s^2 + 445s + 98700}$ is the fin servo dynamics, $H_r(s) = \frac{253000}{s^2 + 710s + 253000}$ is the rate gyro dynamics, and $H_{a_y}(s) = \frac{394800}{s^2 + 890s + 394800}$ is the lateral accelerometer dynamics. The accelerometer is placed at a position displaced from the missile's c.g., 0.7 m aft the nose. This produces measured

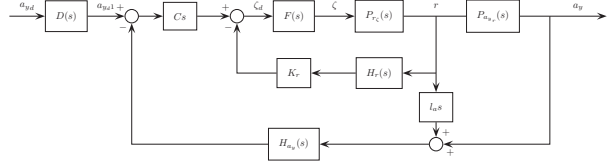


Fig. 2. 2 DOF autopilot configuration.

acceleration a_{y_m} that contains component of angular acceleration of

$$a_{y_m} = a_y + l_a \dot{r}, \quad (6)$$

where l_a is the accelerometer moment arm from the c.g. The control structure incorporates a lag-lead in the error limb and is closed around acceleration feedback with body rate feedback used to improve the closed-loop stability. With an additional prefilter, there is no direct relationship the stability margins of the feedback system and its time-domain response (in practice, it is very important to have it). The autopilot is designed by setting K_r the gyro gain, $C(s)$ the lag-lead compensator and $D(s)$ the prefilter to have acceptable closed-loop frequency-domain tracking performances.

Define $P_{a_{y_r}}(s) = a_y(s)/r(s)$, $G(s) = -C(s)F(s)/(1 - K_r F(s)P_{r_\zeta}(s)H_r(s))$, and $H(s) = (l_a s P_{a_{y_r}}^{-1}(s) + 1)H_{a_y}(s)$. The following key transfer functions will be used throughout:

1. The open loop transfer function

$$L(s) = G(s)P(s)H(s). \quad (7)$$

2. The sensitivity function

$$S(s) = \frac{1}{1 + L(s)}. \quad (8)$$

3. The tracking transfer function

$$T(s) = D(s)G(s)P_{a_{y_\zeta}}(s)S(s). \quad (9)$$

1.4 Closed-Loop Performance Specifications

The autopilot is required to track a lateral acceleration demand a_{y_d} over the whole flight envelope (the Mach number is seen to range from 1.8 to 3.9), where $|a_{y_d}| \leq 500$ m/s² is constrained by limitations on the airframe's structural integrity. It must also be as robust to the variation in fuel state and airframe parameter estimation errors ($\Delta x_{cp}, \Delta C_{y_v}, \Delta C_{y_\zeta}, \Delta C_{n_r} = \pm 5\%$). A list of performance specifications (for a step input) is given in the mixed time- and frequency-domain using familiar figures as follows:

1. Bandwidth $\omega_{-3 \text{ dB}} = 40$ rad/s.
2. Settling time variation $|\delta t_s| \leq 0.05$ s.
3. Steady state error $e_{ss} \leq 10\%$.
3. Damping ratio $0.6 \leq \zeta_{a_y} \leq 1.0$.
4. Gain margin $GM \geq 9$ dB, Phase margin $PM \geq 40^\circ$.

2. DESIGN OF LATERAL MISSILE AUTOPILOT

2.1 Operating Regime Approach

Recall that the missile autopilot must produce the correct control characteristics over a wide range of operating conditions which effect aerodynamic characteristics. However it is usually impossible to design a LTI feedback system to achieve this. Of course, with the non-linear controller whose parameters are functions of the operating points, the design problem is much more difficult. Nevertheless, the operating regime based approach, where a number of standard LTI controllers are designed to meet the desired stability, performance and robustness criteria locally, offers an engineering-friendly solution to this design problem.

Using the data of section 1.1, the lateral acceleration transfer function (5) can be approximated to

$$P_{a_{y\zeta}}(s) \approx \frac{-Un_{\zeta}y_v}{s^2 + Un_v} \quad (10)$$

(Horton, 1995). We take an ad-hoc approach to the decomposition of operating envelope. It is desired that the operating regions are overlapped, and the migration of parameterised variables from one operating region to another is as small as possible. Further observation shows that the contours of surface $-Un_{\zeta}y_v$ can be closely approximated by a set of parallel straight lines (see figure 3). Similar results are found for Un_v . However, the resulting slopes for both $-Un_{\zeta}y_v$ and Un_v are different.

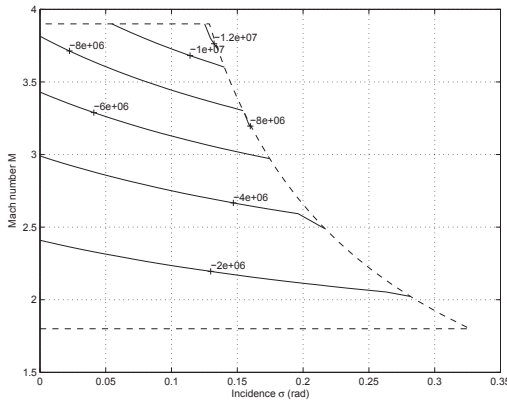


Fig. 3. Contours of $-Un_{\zeta}y_v$.

Suppose a number of partitions is by trial and error given, says 9. From figure 3, it is possible to partition the operating envelope with a set of 9 parallel lines that minimises the migration of both $-Un_{\zeta}y_v$ and Un_v from one operating region to another. However, the compromise solution is to be expected as the gradients of $-Un_{\zeta}y_v$ and Un_v are different. In this study, the difference is measured in logarithmic space. Using an optimisation algorithm described in section 3.1, the optimum decomposition is shown in figure 4. Note

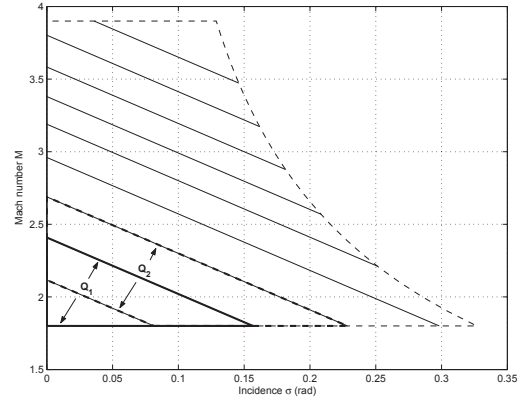


Fig. 4. Decomposition of operating envelope.

that if the design is not feasible, the operating envelope will need to be repartitioned.

2.2 Measures of Performance

2.2.1. Stability Requirements

Asymptotic Stability

The stability of the closed-loop system can graphically be checked using the Nyquist plot or Nichols chart. However, it is numerically difficult. In this paper, the stability of the closed-loop system is simply determined by solving the roots of the characteristic polynomial. The function

$$C_0 = \begin{cases} 0 & \text{if } S(s) \text{ is asymptotically stable,} \\ 1 & \text{otherwise,} \end{cases} \quad (11)$$

Right Half Plane Pole-Zero Cancellation

To ensure internal stability, we must guarantee not only stability of $S(s)$ but also that there is no RHP pole-zero cancellation when $L(s)$ is formed. One way to achieve this is it is desired that minimum phase and stable controller $C(s)$ is designed.

2.2.2. Frequency Domain Performance Requirements

In this paper, the performance specifications are modelled in the frequency domain requirements which have a convenient graphical interpretation in terms of tracking ratios. With the design objectives given in section 1.4, the controller's performances can then be measured by evaluating the following robustness assessment functions:

Gain and Phase Margins

A look at the inverted Nichols chart in figure 5 qualitatively reveals that gain and phase margins decrease as the values of the contours of constant $|S(j\omega)|$ increases. For instance, if $|S(j\omega)| \leq 3$ dB, then $GM > 10$ dB and $PM > 40^\circ$ are guaranteed. (Sidi, 2001)

Adopting these relationships, the gain-phase margin based cost function can be given by

$$J_1 = \max_{\omega} \frac{|S(j\omega)| - M_0}{M_r - M_0}, \quad (12)$$

3. EA-BASED CONTROLLER DESIGN

3.1 Multi-Objective Evolutionary Optimisation Algorithm

Basic scheme of the multi-objective evolution strategy (($\mu + \lambda$)-ES) used in this paper is as that described in (Deb, 2001). Instead of, using non-dominated ranking, finding all Pareto solutions, it locates some specific solutions on the Pareto front corresponding to a given set of target vectors (e.g. weighted Min-Max) $V = \{\mathbf{v}_1, \dots, \mathbf{v}_T\}$ (Hughes, 2003). Each generation, T weighted Min-Max distances are evaluated for all $\mu + \lambda$ solutions, whose results are held in a matrix $S = (s_{ij})$. Note that

$$s_{ij} = \max_{j=1, \dots, 4} w_j^{(k)} O_i^{(k)}, \quad (14)$$

where $w_j^{(k)} = 1/v_j^{(k)}$ and $O_i^{(k)}$ is i^{th} individual's k^{th} objective value. Each column of the matrix S is then ranked, with the best score population member on the corresponding target vector being given a rank of 1, and the worst a rank of $\mu + \lambda$. The rank values are stored in a matrix R . Now R can be used to rank the population based on the number of target vectors that are satisfied the best.

The primary advantages of this method is such that the target vectors can be arbitrary generated focusing on the interested regions. Also the limits of the objective space and discontinuities within the Pareto set can be identified by observing the distribution of the angular errors ($\theta_i = \cos^{-1} \hat{\mathbf{v}}_j \cdot \hat{\mathbf{O}}_i$) across the total weight set.

3.2 Robust Design Methodology

For each of the 6 operating regions, the employed controller transfer functions are of the forms K_r , $C(s) = K_p \frac{(s+z_p)}{(s+p_p)}$ and $D(s) = \frac{K_d}{s+p_d}$. The optimisation variables straightforwardly are K_r , K_p , z_p , p_p , K_d and p_d . Likewise classical loop-shaping, these set of parameters are then translated into the logarithmic space, thus

$$\mathbf{x} = [\bar{K}_r, \bar{K}_p, \bar{z}_p, \bar{p}_p, \bar{K}_d, \bar{p}_d], \quad (15)$$

where $\bar{K}_r = \log_{10} K_r$, $\bar{K}_p = \log_{10} K_p$, etc..., is now formed a variables vector for the ES. This allows quite large ranges of all the parameters to be explored, and proves to speed up the convergence of the ES (Chen and Ballance, 1999).

It has to be noted that robustness analysis of an uncertain system can be computationally very expensive. In fact, (Ackermann *et al.*, 1993) states that using the vertex points is enough in robust controller design for most practical systems. To reduce the computational cost, the similar optimisation process as describe in (Söylemez, 1999) is followed, where addition vertices are added in each loop until an optimal solution satisfies the search criteria.

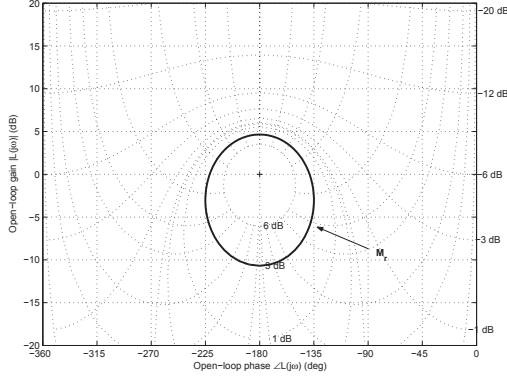


Fig. 5. Inverted Nichols chart.

where $M_0 = -6$ dB, and M_r is the admissible resonant peak of the sensitivity function $S(j\omega)$.

Tracking Error

The system's tracking performance specifications are based upon satisfying all of the frequency forcing functions $|B_U(j\omega)|$ and $|B_L(j\omega)|$ shown in figure 6a. They represent the upper and lower bounds of track-

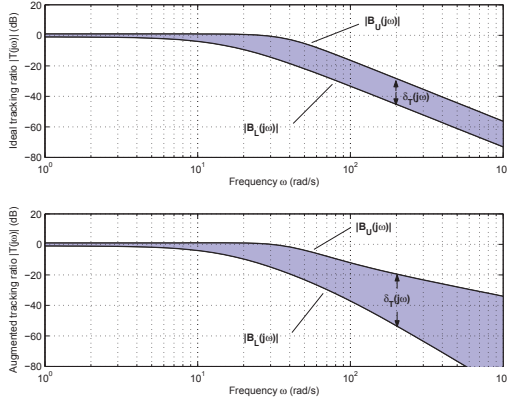


Fig. 6. Ideal and augmented tracking models.

ing performance specifications whom an acceptable response $|T(j\omega)|$ must lie within. However, the difference between $|B_U(j\omega)|$ and $|B_L(j\omega)|$ is required to increase with increasing frequency. This can be achieved by augmenting $B_U(s)$ with a zero as close to the origin as possible without significantly affecting the time response (see figure 6b). The spread can be further increased by similarly augmenting $B_L(s)$ with a real negative pole. (Houpis and Rasmussen, 1999)

Following this design concept, the tracking boundaries based cost function can be defined by

$$J_2 = \max_{\omega} \left\{ \frac{|T(j\omega)| - |T_0(j\omega)|}{|B_U(j\omega)| - |T_0(j\omega)|}, \frac{|T_0(j\omega)| - |T(j\omega)|}{|T_0(j\omega)| - |B_L(j\omega)|} \right\}, \quad (13)$$

where $|T_0(j\omega)|$ is the nominal tracking model.

3.3 Controller's Parameters Tuning

Consider the operating region Q_5 in figure 4. Pursuing the method described in section 3.1 (using (100+100)-ES), the Pareto-optimal solutions corresponding to a given set of weight vectors ($0.1 \leq w^{(k)} \leq 1.0$) are shown in figure 7, where the limits and discontinuities

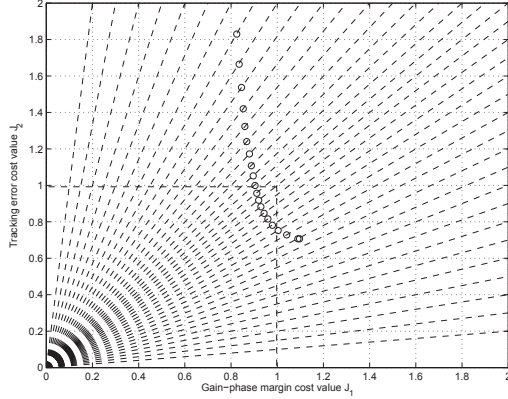


Fig. 7. Pareto-optimal solutions for the given control structure.

within the Pareto set are indicated by where the solutions are missing. In this case, 7 runs are needed which results in the total 28 vertices used in the optimisation process.

The trade-offs can now be analysed in which the preferred solution will depend on the designer choice. Suppose the unity weighted min-max solution is chosen as a decision choice. The results corresponding to the minimising objectives are shown in figure 8 and 9. These reveal that the controller is locally a robust controller for all perturbation vertices. The step response

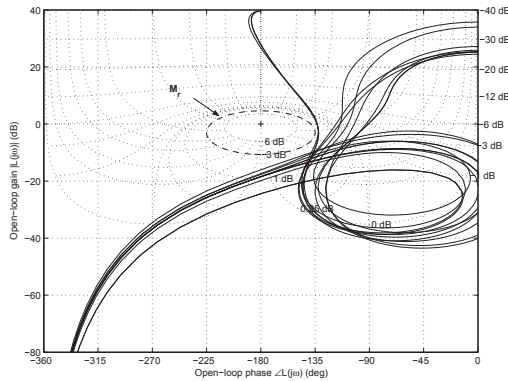


Fig. 8. Open-loop frequency response $L(j\omega)$.

of the selected vertex systems are shown in figure 10.

4. ROBUST GAIN-SCHEDULED CONTROLLER

4.1 Fuzzy Membership Function

It is not natural to have a sudden change between the operating regimes. In this paper, a smooth deterministic transition between the operating regimes is

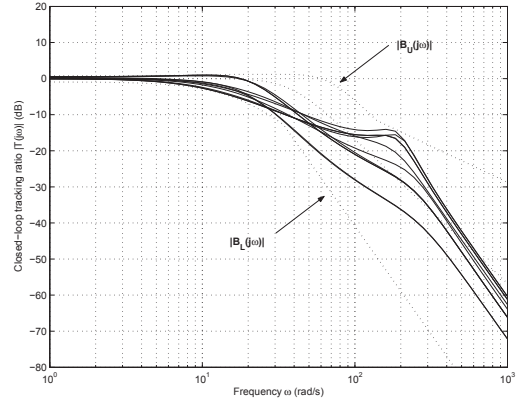


Fig. 9. Closed-loop frequency response $|T(j\omega)|$.

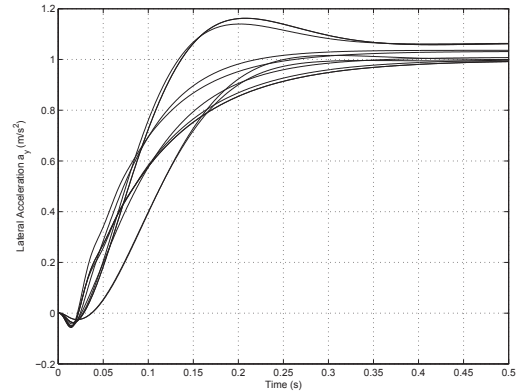


Fig. 10. Step response of the vertex systems.

implemented based on the framework of fuzzy sets and fuzzy logic. Recall that the operating regions are partitioned using a set of parallel straight lines (see figure 4). Thus, 9 corresponding fuzzy sets can be parameterised by the vector component of the operating point along the vector orthogonal to those lines. For simplicity in implementation, the triangular membership functions are used and arranged by Ruspini-type partition keeping the sum of the membership degrees equal to 1 as shown in figure 11.

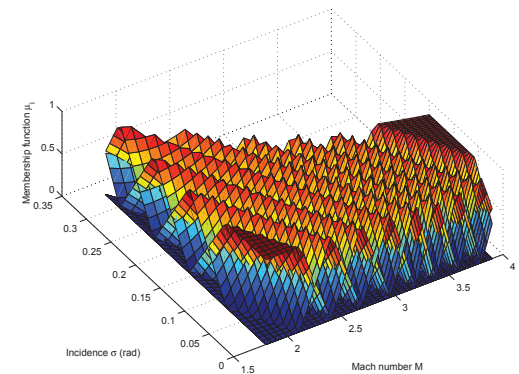


Fig. 11. Membership functions associated with Mach number and incidence.

4.2 Takagi-Sugeno Fuzzy Interpolation

Following the design used in section 3.3, the optimal controllers are obtained for each 9 operating regions. In this paper, direct linear interpolation of zeros, poles and gains is implemented. This is feasible as the migration of poles and zeros (of the same weight vector) from one to the next is clearly recognisable in this case. Note also that the interpolation of zeros, poles and gains usually provides smoother and more robust control than the interpolation of polynomial coefficients in rational transfer functions (Murray-Smith and Johansen, 1997).

In this case, the fuzzy inference rule can be represented as a zero-order TS fuzzy model of the form

$$R_i : \text{If } x_i \text{ is } A_i \text{ then } K_r = K_{r_i}, K_p = K_{p_i}, \text{etc.} \dots, (16)$$

where R_i denotes the i th rule, $i = 1, \dots, 6$, x is the vector of operating conditions, and A is the fuzzy set described in section 4.1. Based on product-sum-gravity at a given input, the final outputs of the fuzzy model are given by

$$K_r = \frac{\sum_{i=1}^6 \mu_i(x) K_{r_i}}{\sum_{i=1}^6 \mu_i(x)}, \quad (17)$$

where the weight, $0 \leq \mu_i(x) \leq 1$, represents the degree of membership defined in figure 11. K_p , z_1 , etc... are similar.

Employing the non-linear 2 DOF model described in section 1.1, the time responses of the TS fuzzy interpolated controller is shown in figure 12. The

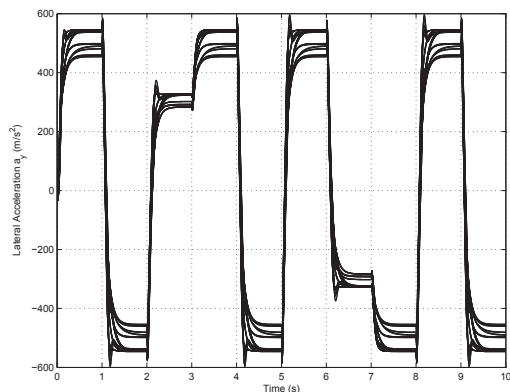


Fig. 12. Lateral acceleration sequence step response of the perturbation vertex systems.

simulation results show that the resulting controller is a robust tracking gain-scheduling controller for at least all the perturbation vertices.

5. CONCLUSION

This paper presents the design procedure for the lateral acceleration missile autopilot using the multi-objective evolutionary optimisation method. A decomposition of the operating envelope based on the

dominated parameters is used in which the resulting number of partitions becomes transparent.

The closed-loop performance specifications are transformed into the frequency domain requirements which can conveniently be interpreted graphically. The design is then reduced to an optimisation problem which can straightforwardly be solved using the evolution strategy based on the proposed cost and constraint formulations. The Pareto-optimal solutions of the LTI controller are determined corresponding to the given target vectors. It is shown that the selected controller is locally a robust controller for all possible perturbations.

The smooth deterministic transition between the operating regimes is implemented using the zero-order TS fuzzy model, where the controller's zeros, poles and gains are the fuzzy consequent. The non-linear simulation results show that the interpolated controller is a robust tracking controller for at least all the perturbation vertices.

REFERENCES

- Ackermann, J., A. Bartlett, D. Kaesbauer, W. Sienel and R. Steinhauser (1993). *Robust Control: Systems with Uncertain Physical Parameters*. Springer.
- Chen, W. H. and D. J. Ballance (1999). Genetic algorithms enabled computer-automated design of QFT control systems. In: *IEEE International Symposium on Computer Aided Control System Design*. Hawaii.
- Deb, K. (2001). *Multi-Objective Optimization using Evolutionary Algorithms*. John Wiley and Sons.
- Horton, M. P. (1992). A study of autopilots for the adaptive control of tactical guided missiles. Master's thesis. University of Bath. Bath, UK.
- Horton, M. P. (1995). Autopilots for tactical missiles: An overview. *IMechE: Journal of Systems and Control Engineering* **209**, 127–139.
- Houpis, C. H. and S. J. Rasmussen (1999). *Quantitative Feedback Theory: Fundamentals and Applications*. Marcel Dekker.
- Hughes, E. J. (2003). Multiple single objective pareto sampling. In: *the Congress on Evolutionary Computations*. Canberra.
- Murray-Smith, R. and T. A. Johansen (1997). *Multiple Model Approaches to Modelling and Control*. Taylor and Francis.
- Sidi, M. (2001). *Design of Robust Control Systems: From Classical to Modern Practical Approaches*. Krieger.
- Söylemez, M. T. (1999). *Pole Assignment for Uncertain Systems*. Research Studies Press.